Optimal Dual-VENC (ODV) Unwrapping in Phase-Contrast MRI

Hugo Carrillo, Axel Osses, Sergio Uribe, Cristobal Bertoglio

Optimal Dual-VENC (ODV) Unwrapping in Phase-Contrast MRI

Hugo Carrillo[a], Axel Osses[a,b], Sergio Uribe[b,c,d,*], Cristóbal Bertoglio[e,*]

[a]*Center for Mathematical Modeling, Universidad de Chile, Chile*
[b]*Millennium Nucleus for Cardiovascular Magnetic Resonance*
[c]*Center for Biomedical Imaging, Pontificia Universidad Católica, Chile*
[d]*Radiology Department, School of Medicine, Pontificia Universidad Católica, Chile*
[e]*Bernoulli Institute, University of Groningen, The Netherlands*

***Abstract*—Dual-VENC strategies have been proposed to improve the velocity-to-noise ratio in Phase-Contrast MRI. However, they are based on aliasing-free high-VENC data. The aim of this work is hence to propose a dual-VENC velocity estimation method allowing high-VENC aliased data. For this purpose, we reformulate the phase-contrast velocity as a least squares estimator, providing a natural framework for including multiple encoding gradient measurements. By analyzing the mathematical properties of both single- and dual-VENC problems, we can justify theoretically high/low-VENC ratios such that the aliasing velocity can be minimized. The resulting reconstruction algorithm was assessed using three types of data: numerical, experimental and volunteers. In clinical practice, this method would allow shorter examination times by avoiding tedious adaptation of VENC values by repeated scans.**

***Keywords*—Phase-Contrast MRI, dual-VENC, unwrapping**

I. Introduction

Velocity-encoded Phase-Contrast MRI (PC-MRI) is a well-established method for measuring flow velocities, with several applications to quantitative analysis of cardiovascular pathologies [1]. The velocity-encoding magnetic gradients are set by the choice of the velocity encoding parameter, or VENC [2]. It is well known that the velocity-to-noise-ratio (VNR) worsens when increasing the VENC. However, if VENC is set lower than the true velocity (which is unknown prior to the scan), velocity aliasing occurs. Moreover, even for VENC values slightly larger than the true velocity, velocity aliasing may occur due to measurement noise. These restrictions promote in clinical practice to acquire images at different VENCs, obligating the MRI operator to manually select the image for one specific VENC, while the aliased images are ignored and the time spent is squandered.

Corresponding author. Email: c.a.bertoglio@rug.nl. Address: Nijenborgh 9, 9747 AG Groningen, The Netherlands

*C.B. and S.U. are both last authors.

Velocity aliasing is one of the main limitations for measuring complex features of blood flows, particularly, when high and low velocities are present in the same image, such as in heart, valvular and vascular malformations.

Then, VENC has to be set high, but as a consequence, low VNR is present in low velocity regions, for instance in recirculation regions in aneurisma or false lumen in dissections, to name a few. This leads to important inaccuracies when further analysis of the flow is performed [3]. Aliasing is also problematic in many PC-MRI techniques, like Tissue Phase Mapping [4] and Elastography [5], where the motions magnitude vary across the regions of interest.

In order to reduce aliasing artefacts, unwrapping algorithms have been developed by assuming that the velocity field is smooth in space and/or time, see e.g. [6] and references therein. Nevertheless, they often fail when the aliased regions are large. Therefore, voxelwise dual-VENC strategies have been proposed, i.e. without any assumption of smoothness of the flow [7], [8], [9], [3], [10]. They have been based on unwrapping low-VENC data by using the high-VENC reconstruction, which is assumed aliasing-free. While actual approaches allow to improve the VNR with respect to a single high-VENC acquisition, they fail when the high-VENC data is aliased. Also, there is a lack of mathematical support for choosing the low- and high-VENCs. All of these issues limits the applicability of dual-VENC techniques, particularly when the peak velocities are uncertain.

Therefore, the aim of this work is to provide a mathematical framework to obtain aliasing-free velocity estimations from dual-VENC data, even when the both VENC acquisitions are aliased. The key is the least-squares formulation of the PC-MRI problem, whose mathematical properties allow to propose optimal combinations of VENCs to achieve this goal. We also present a numerical algorithm for dual-VENC reconstructions, which is successfully applied to numerical, experimental and volunteer data sets.

II. THEORY

A. Classical PC-MRI

Assuming a constant velocity field, the usual starting point of classical PC-MRI is the model for the phase of the transverse magnetization at the echo-time [7]:

$$\varphi^G = \varphi^0 + \vartheta^G \tag{1}$$

with $\varphi^0 \in [0, 2\pi)$ the reference phase, and

$$\vartheta^G = \vartheta^G(u) = \gamma u M_1(G) \tag{2}$$

the velocity dependent phase. Here, $u \in \mathbb{R}$ the flow velocity component parallel to the velocity-encoding gradient $G = G(t) \in \mathbb{R}$, with t the encoding time, and $M_1(G) \in \mathbb{R}$ the first-order moment of $G(t)$. The constat $\gamma > 0$ is the giromagnetic ratio.

From now on, we deal with different gradients G_i with different amplitudes. Assuming that we have measured two phases φ^{G_0} and φ^{G_1} with $G_0 \neq G_1$, the *phase-contrast* velocity is estimated by

$$u_{pc} := \frac{\varphi^{G_0} - \varphi^{G_1}}{\pi} \text{VENC}(G_0, G_1), \tag{3}$$

with

$$\text{VENC}(G_0, G_1) = \frac{\pi}{\gamma(M_1(G_0) - M_1(G_1))}.$$

In the case that the true velocity $|u_{true}| \leq |\text{VENC}|$, then $u_{pc} = u_{true}$. But if $|u_{true}| > |\text{VENC}|$, the phase difference exceeds $\pm\pi$ and aliasing occurs, i.e. $u_{true} \neq u_{pc}$. However, increasing the VENC decreases the VNR. Therefore, choosing the VENC parameter is an iterative manual process trying to set it as small as possible to maximize VNR and at the same time large enough to avoid aliasing.

B. Dual-VENC approaches

It is well known that for any VENC value, u_{true} belongs to the set of infinite but numerable solutions of type

$$u_{pc} + 2k\text{VENC}(G_0, G_1), \;\; k \in \mathbb{Z}. \tag{4}$$

Therefore, it is natural to extend the velocity estimation problem such that k can be also estimated using additional encoding gradient measurements.

Assuming that now three measurements with gradients $G_0 = 0 < G_1 < G_2$ are available, two velocities at different VENC values can be reconstructed: the phase-contrast velocity u_1 at $\text{VENC}_1 = \text{VENC}(G_1, 0)$ and a set of velocities $u_2 + 2k\text{VENC}_2$ at $\text{VENC}_2 = \text{VENC}(G_2, 0)$, with $\text{VENC}_1 > \text{VENC}_2$, $k \in \mathbb{Z}$. Standard dual-VENC unwrapping strategies, see e.g. [10], [7], aim to find the correct low-VENC velocity from an un-aliased high-VENC velocity u_1. Hence, an improved VNR should be achieved. Here, we will compare our new dual-VENC approach against the one from [10], which is defined as:

$$u_{\text{SDV}} = \begin{cases} u_2 + 2 \cdot \text{VENC}_2 & \text{if } \epsilon_1 < D < \epsilon_2 \\ u_2 - 2 \cdot \text{VENC}_2 & \text{if } -\epsilon_2 < D < -\epsilon_1 \\ u_2 + 4 \cdot \text{VENC}_2 & \text{if } \epsilon_3 < D < \epsilon_4 \\ u_2 - 4 \cdot \text{VENC}_2 & \text{if } -\epsilon_4 < D < -\epsilon_3 \end{cases}$$

with $D = u_1 - u_2; \epsilon_1 = 1.6 \cdot \text{VENC}_2; \epsilon_2 = 2.4 \cdot \text{VENC}_2;$ $\epsilon_3 = 3.2 \cdot \text{VENC}_2; \epsilon_4 = 4.8 \cdot \text{VENC}_2$. In the reminder of this article, we will denote it as *standard* dual-VENC (SDV).

Note that the SDV reconstruction will be aliased if $|\text{VENC}_1| < |u_{true}|$. The new dual-VENC method based on our analysis will overcome this issue by optimally choosing both VENC_1 and VENC_2 based on a reformulation of the phase-contrast problem presented next.

C. Least-squares formulation of the single-VENC problem

For a given velocity encoding gradient G let us denote the measured phase of transverse magnetization by $\hat{\varphi}^G$.

Assume now that we have available two measurements: a reference one for $G = 0$, and another for $G \neq 0$. We formulate the velocity reconstruction as a standard maximum-likelihood estimation problem from the phase measurements, by means of the least-squares function

$$\begin{aligned} J_G(u) &= \frac{1}{2}\Big(\cos(\hat{\vartheta}^G) - \cos(\vartheta^G(u))\Big)^2 \\ &\quad + \frac{1}{2}\Big(\sin(\hat{\vartheta}^G) - \sin(\vartheta^G(u))\Big)^2 \qquad (5) \\ &= \Big(1 - \cos\left(\hat{\vartheta}^G - \vartheta^G(u)\right)\Big) \qquad (6) \end{aligned}$$

with $\hat{\vartheta}^G = \hat{\varphi}^G - \hat{\varphi}^0$ the "measured" velocity dependent phase.

Least-squares formulations have also been recently applied in the context of unwrapping methods using the information of contiguous voxels for various types of single- and dual-VENC acquisitions [11]. However, no analysis of their properties or potential for optimizing the VENC combinations was reported.

Figure 1 shows examples of the functions $J_G(u)$, for different gradients represented by $\text{VENC}(G, 0)$. The synthetic measurements were generated with a unitary magnitude and the phases from Equation (1) using $\varphi^0 = \gamma B t_E$ with $B = 1.5\ T$, $\gamma = 267.513e3\ rad/T/ms$, $t_E = 5\ ms$, a velocity $u_{true} = 1\, m/s$. It can be appreciated that the functions are periodic, with the period depending on the VENC, and also that the true velocity is a local minimum independent on the VENC. The following propositions proof these observations.

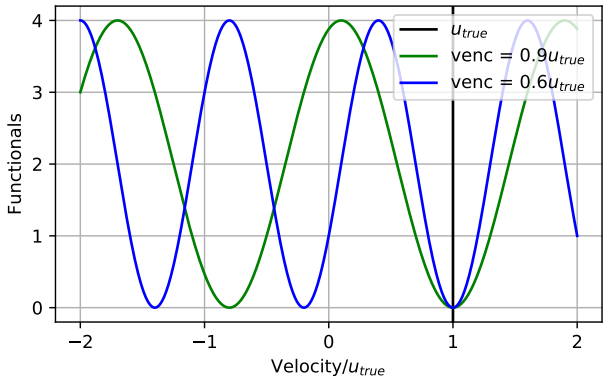

Fig. 1. cost functions $J_G(u)$ for u_{true} and two VENC values.

Proposition 1: $J_G(u)$ is a periodic function with period $2\text{VENC}(G,0)$.

Proof: It suffices to see that the cosine and sine are 2π-periodic functions, and

$$\begin{aligned}\vartheta^G(u+2\text{VENC}(G,0)) &= \gamma(u+2\text{VENC}(G,0))M_1(G)\\ &= \gamma u M_1(G)+2\pi\\ &= \vartheta^G(u)+2\pi\end{aligned}$$

■

Proposition 2: The critical points u_k of $J_G(u)$ are

$$u_k = \frac{\hat{\varphi}^G-\hat{\varphi}^0}{\gamma M_1(G)} + k\text{VENC}(G,0)\ ,\ k\in\mathbb{Z} \tag{7}$$

Proof: From (6) we see that

$$\frac{\partial J_G}{\partial u} = -\gamma M_1(G)\sin(\hat{\vartheta}^G-\vartheta^G). \tag{8}$$

At the critical points we must then have:

$$\sin(\hat{\vartheta}^G-\vartheta^G)=0 \Longleftrightarrow \vartheta^G(u_k)=\hat{\vartheta}^G+k\pi,\quad k\in\mathbb{Z}. \tag{9}$$

Finally, using Equation (2) we obtain

$$u_k = \frac{\hat{\varphi}^G-\hat{\varphi}^0}{\gamma M_1(G)} + k\frac{\pi}{\gamma M_1(G)}. \tag{10}$$

■

Proposition 3: At the critical points of $J_G(u)$, the second derivatives are given by

$$\frac{\partial^2 J_G}{\partial u^2}(u_k) = C\cdot(-1)^k,\ k\in\mathbb{Z}, C>0.$$

Proof: Taking the derivative in (8) we obtain:

$$\frac{\partial^2 J_G}{\partial u^2}(u_k) = \gamma^2 M_1(G)^2\cos(\hat{\vartheta}^G(u_k)-\vartheta_u^G) = C\cdot(-1)^k \tag{11}$$

where the last equality holds due to Equation (9). ■

In conclusion, we have just proved that Equation (4) corresponds to the local minima of the cost function J_G by taking k as an even number in Equation (11).

It is also straightforward to show that the true velocity u_{true} belongs to the set of local minima of J_G when the measurements are noise-free. Indeed, in that case $\hat{\varphi}^G = \hat{\varphi}^0+\gamma M_1(G)u_{true}+2k\pi$, and if we choose $\varphi^G(u_{true}) = \hat{\varphi}^0+\gamma M_1(G)u_{true}$, then $J_G(u_{true})=0$ from Equation (6).

D. The dual-VENC least squares problem

We assume now that we have measured the magnetization vector with three encoding gradients $G_0=0<G_1<G_2$. We can then define the dual-VENC least squares sum function as:

$$J_\Sigma(u) = \sum_{i=1}^{2}\left(1-\cos\left(\hat{\vartheta}^{G_i}-\vartheta^{G_i}(u)\right)\right)$$

Figure 2 shows the single- and dual-VENC least-squares functions for different VENC combinations $\text{VENC}_1 > \text{VENC}_2=\beta\text{VENC}_1$, $0<\beta<1$. Hence, the VENCs can be set in terms of VENC_1 and β. Note that VENC_1 is set lower than u_{true} and is kept fixed in all plots, while β is variable. We can first observe that in all cases local and global minima are present in the dual-VENC functions $J_\Sigma(u)$. However, the true velocity is always a global minimum since it is a local and global minimum for each VENC, as shown in the previous section.

Remarkably, the periodicity of J_Σ is now the least common multiplier (lcm) between the periodicity of the single-VENC functions, i.e. $L_\Sigma := \text{lcm}(2\text{VENC}_1,\ 2\text{VENC}_2)$. As a consequence, if β is carefully chosen, e.g. in Figure 2(a) and 2(b), J_Σ has a larger period than the original single-VENC functions, namely $L_\Sigma > 2\text{VENC}_1$. Therefore, even though $\text{VENC}_1, \text{VENC}_2 < |u_{true}|$, we can still distinguish u_{true} from the other global minima since they have larger absolute values.

However, if we do not choose β well, e.g. as in Figures 2(c) and 2(d), then $L_\Sigma = 2\text{VENC}_1$ and the global minima with smallest absolute value will not be u_{true} if $\text{VENC}_1 < u_{true}$ and velocity aliasing occurs.

A general method for computing the aliasing limit is: for $\beta=\alpha/\alpha_0$, with $\alpha,\alpha_0\in\mathbb{N}$ the smallest possible values, then it is easy to verify that the periodicity of J_Σ is $L_\Sigma=\alpha 2\text{VENC}_1$, since

$$L_\Sigma = k_1 2\text{VENC}_1 = k_2 2\beta\text{VENC}_1,\ k_1,k_2\in\mathbb{Z}$$

leading to $k_1=\alpha$, $k_2=\alpha_0$. Then, aliasing will occur when $||u_{true}|-L_\Sigma/2|<|u_{true}|$, i.e. $\text{VENC}_1<|u_{true}|/\alpha$.

Table I gives examples of VENC_1 such that the global minimum of J_Σ with lowest magnitude corresponds to u_{true} depending on β.

β	0.95	0.9	0.75	0.7	0.66	0.55	0.5
α	19	9	3	7	2	11	1

TABLE I. EXAMPLES OF ALIASING LIMITS FOR DECREASING VALUES OF β. ODV METHOD ALLOWS ALIASING-FREE ESTIMATION IF $\text{VENC}_1 > |u_{true}|/\alpha$.

E. Choice of β

As shown in Table I, in the case without any measurement noise, to maximize the periodicity of J_Σ one should choose $\text{VENC}_2 \approx \text{VENC}_1$, making the aliasing velocity very small, or for instance $\beta=0.7$ or $\beta=0.55$ as indicated in Table I.

However, the presence of noise deforms the dual-VENC functions, see Figure 3, since the noise is independent for each VENC. Therefore, local minima from both single-VENC cost functions that are not necessarily u_{true} can get close to each other. Hence, there is an increased risk for u_{true} not being global minima when α is large. In order to maximize the robustness to noise, the local minima of both single-VENC functions should be separated as much as possible. As shown in Figure 2(b), this is indeed the case for $\beta=0.66$. For $\beta=0.75$ this separation is less pronounced, however $\beta=0.75$ would allow to lower the aliasing velocity if noise is low. In general, the optimal choice of β should be optimized to the SNR of the specific MRI scanner, but $\beta=0.66$ is always the most robust to noise due to the largest separation between minima. In the experiments, we will use these two values, $\beta=0.66$

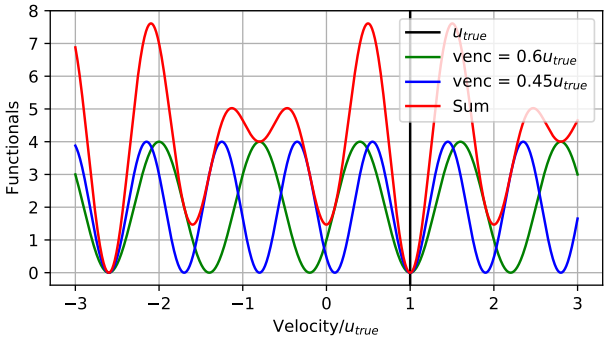

(a) $\beta = 0.75$

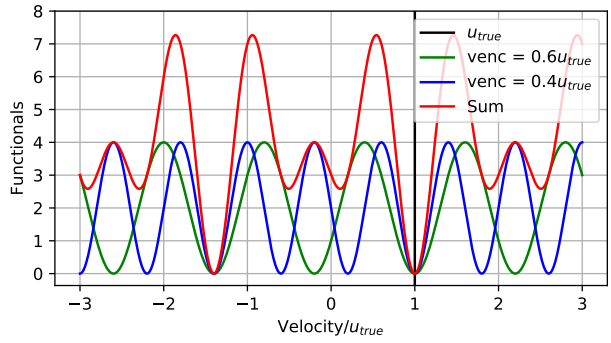

(b) $\beta = 0.66$

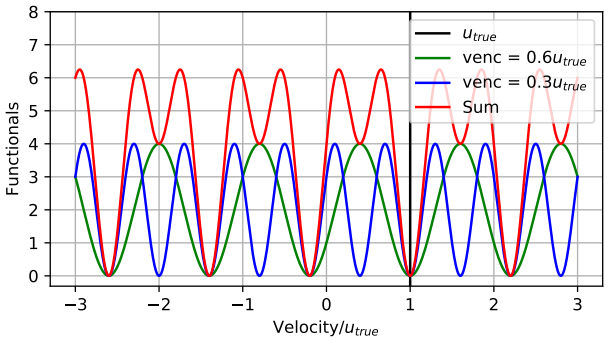

(c) $\beta = 0.5$

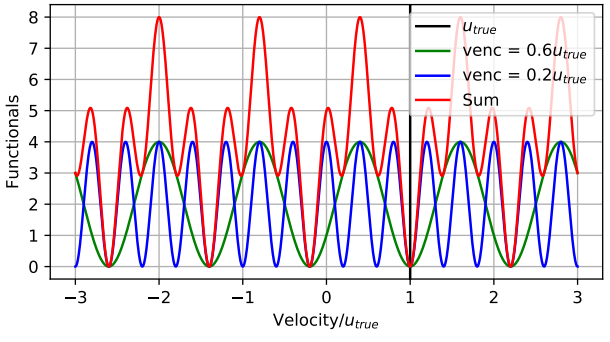

(d) $\beta = 0.33$

Fig. 2. Cost functions $J_G(u)$ and $J_\Sigma(u)$ for different $\text{VENC}_1, \text{VENC}_2 = \beta\text{VENC}_1$.

and $\beta = 0.75$. Additionally, in the experiments with numerical data, we will show the poor performance of $\beta = 0.7$ when noise is present.

F. The optimal dual-VENC (ODV) algorithm

Based on the considerations above, we now detail the ODV velocity estimation algorithm. For the given user-defined parameters VENC_1 and $\text{VENC}_2 = \beta\text{VENC}_1$, $0 < \beta < 1$:

1) Measure phases $\hat{\varphi}^{G_i}$ for three gradients: $G_0 = 0$ and G_1, G_2 such that $\text{VENC}(G_1, 0) = \text{VENC}_1$ and $\text{VENC}(G_2, 0) = \text{VENC}_2$.
2) Find the global minima u_k^*, $k \in \mathbb{Z}$:

$$u_k^* = \underset{u \in [-u_{max}, u_{max}]}{\operatorname{argmin}} J_\Sigma(u),$$

with $u_{max} = \text{lcm}(2\text{VENC}_1, 2\text{VENC}_2)/2$. The estimated dual-VENC velocity corresponds to u_k^* with smallest absolute value.

III. Methods

This section summarizes setups with three types of data: synthetic, phantom and volunteer. In all cases we applied the formula (3) for single-VENC and dual-VENC with both standard [10] (SDV) and new ODV methods. For the ODV algorithm, the global minima was found using a sampling of the cost function J_Σ with uniform spacing of the velocity of $\text{VENC}_2 \cdot 10^{-3}$, which was found to be small enough to avoid numerical artefacts in the global optimization.

A. Synthetic data

The reference phase is defined as $\varphi^0 = \gamma B_0 t_E$ with $B_0 = 1.5\ T$, $\gamma = 267.513e3\ rad/T/ms$, $t_E = 5\ ms$. For the phases of the non-zero flow encoding gradients, we consider $\varphi^{G_{1,2}} = \varphi^0 + u_{true}\pi/\text{VENC}_{1,2}$, with $u_{true} = 1m/s$. Using these phases, reference magnetization measurements were built assuming a unitary magnitude. The estimation is shown in terms of VENC_1 and $\text{VENC}_2 = \beta\text{VENC}_1$, with $\beta = \{0.66, 0.7, 0.75\}$.

We also compute estimations using magnetization measurements perturbed with an additive Gaussian noise with zero-mean and standard deviation of 20% of the magnitude. We express these results in terms of mean estimated velocity for 2000 realizations of the noise and twice the standard deviation.

B. Phantom data

In order to preliminary assess the ODV we used a flow phantom that consisted of a rigid straight hose of 15mm internal diameter, 25mm external diameter. The hose was connected to a MRI-compatible flow pump (CardioFlow 5000 MR, Shelley Medical Imaging Technologies, London, ON, Canada) with a constant flow rate of 200 mL/s. The system was filled with a blood-mimicking fluid (40% distilled H2O, 60% Glycerol) and the set up was similar as in [12], [13]. The MRI data sets were acquired on a clinical 1.5T Philips Achieva scanner (Philips, Best, The Netherlands). The protocol

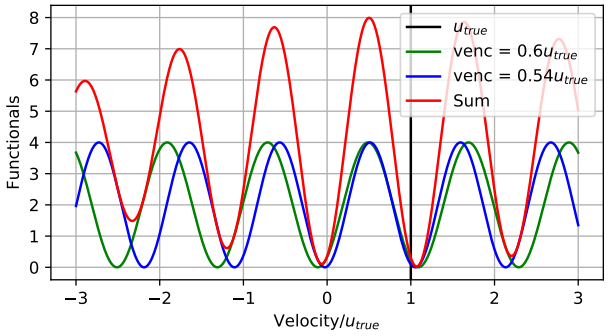

(a) $\beta = 0.9$

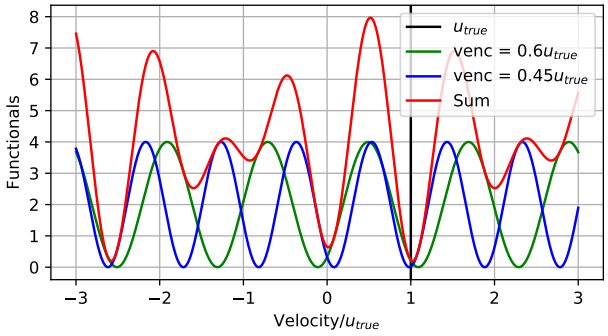

(b) $\beta = 0.75$

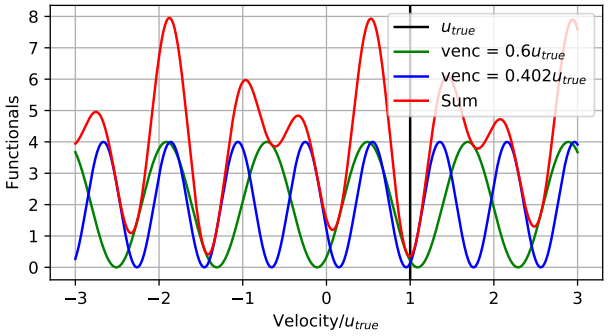

(c) $\beta = 0.667$

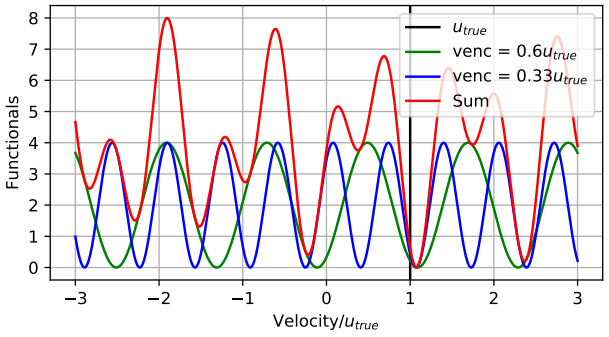

(d) $\beta = 0.55$

Fig. 3. Cost functions $J_G(u)$ for different pair of values of VENC and the sum cost function J_Σ with noisy magnetization measurements (standard deviation 20% of magnitude).

consisted of through-plane PC-MRI sequence with a single cardiac phase due to constant flow rate. The scan parameters were: in-plane resolution was 1x1 mm with a slice thickness of 8 mm, 1 prospective cardiac phase, FA = 12^o, TR=9.2 ms, TE=4.9 ms, matrix size = (256,256).. The data was acquired using non-symmetric pairs of encoding gradients with VENC $= 150, 100, 70$ cm/s with one surface coil. The acquisitions were performed using single-VENC protocols and the dual-VENC reconstructions were computed using only one of the zero-encoding gradients of the corresponding dual-VENC pair.

C. Volunteer data

Eight healthy volunteers underwent MRI in the same 1.5T Achieva scanner using a 5 elements cardiac coil. The protocol consisted of through-plane PC-MRI sequence perpendicular to the ascending aorta just above the valsalva sinus. We used several VENC values: 33.3, 37.5, 50, 66.7, 75, 100 and 150cm/s. These choices allow to generate dual-VENC reconstructions with both values of $\beta = 0.66$ and $\beta = 0.75$. The raw data was obtained and the reconstruction of each bipolar gradient was performed offline using matlab. Data from the multiple coils were combined using the method proposed in [14]. The data was acquired using the following scan parameters: in-plane resolution was 1x1 mm with a slice thickness of 8 mm, 25 cardiac phases using prospective ECG triggering, FA = 15^o, TR=5.5 ms, TE=3.7 ms, matrix size = (320, 232). Temporal resolution depended on the heart rate of the patients, varying between 35ms to 48 ms.

As in the panthom, the acquisitions were performed using single-VENC protocols. One issue with this approach is that the TE may be different depending in the scan setting, particularly may increase for low VENCs [15]. Since we use only the reference phase of VENC_1, the value of the reference phase used in the dual-VENC reconstructions for VENC_2 was scaled by $T_E^{(2)}/T_E^{(1)}$, with $T_E^{(1)}$ and $T_E^{(2)}$ the echo times given by acquisitions with VENC_1 and VENC_2, respectively. This is justify simply by the knowledge about the reference phase being proportional to T_E [16].

IV. RESULTS

A. Synthetic data

Figure 4 shows the estimated velocity against VENC_1 without noise, confirming the unwrapping properties of both dual-VENC approaches: for SDV aliasing occurs when $\text{VENC}_1 < u_{true}$, and for ODV when $\text{VENC}_1 < u_{true}/2$, $\text{VENC}_1 < u_{true}/7$ and $\text{VENC}_1 < u_{true}/3$ with $\beta = 0.66$, $\beta = 0.7$ and $\beta = 0.75$, respectively.

Similar results for noisy measurements are presented in Figure 5, now including the aforementioned confidence interval. As one expects, the spread of the estimations are lower for $\beta = 0.66$. Moreover, in the single-VENC cases we confirm that aliasing starts even before the theoretical value due to the noise. This is also evident for SDV, while ODV is clearly more robust. We can also see that for ODV and $\beta = 0.7$ the confidence interval does not decrease uniformly with VENC_1

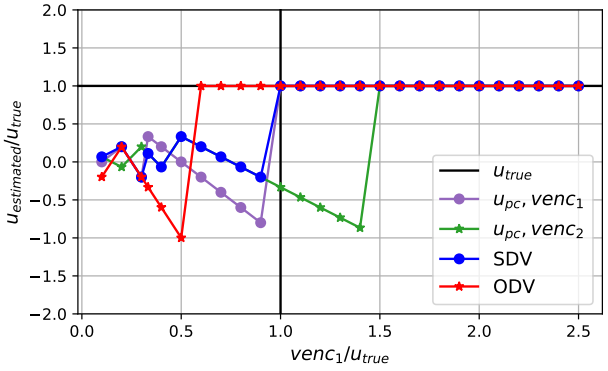

(a) $\beta = 0.667$

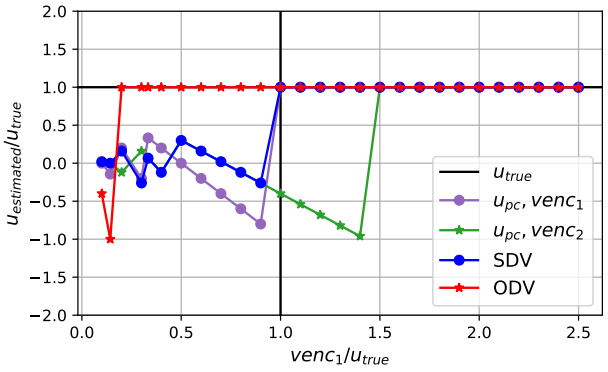

(b) $\beta = 0.7$

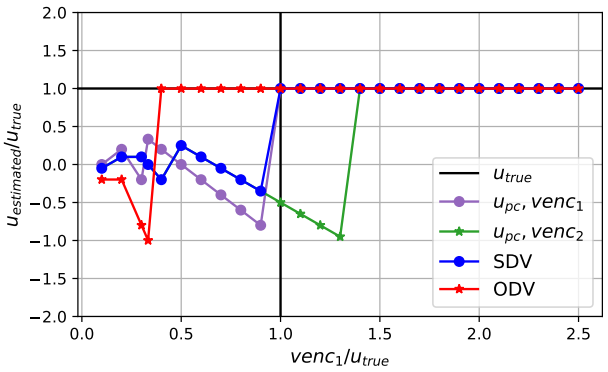

(c) $\beta = 0.75$

Fig. 4. Synthetic data (noise-free): single- and dual-VENC.

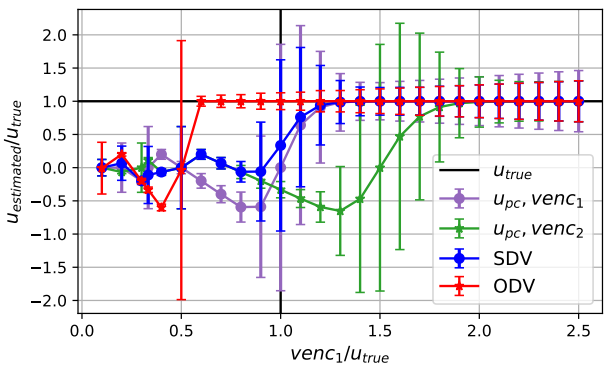

(a) $\beta = 0.667$

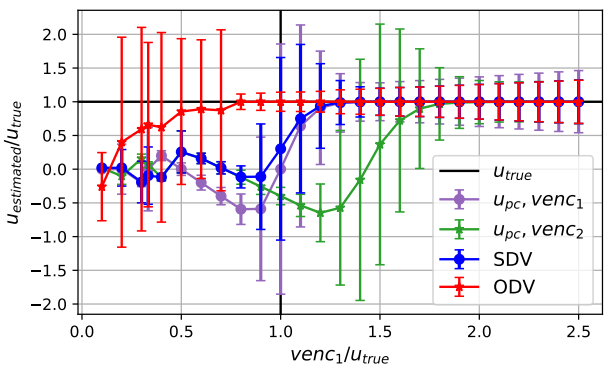

(b) $\beta = 0.7$

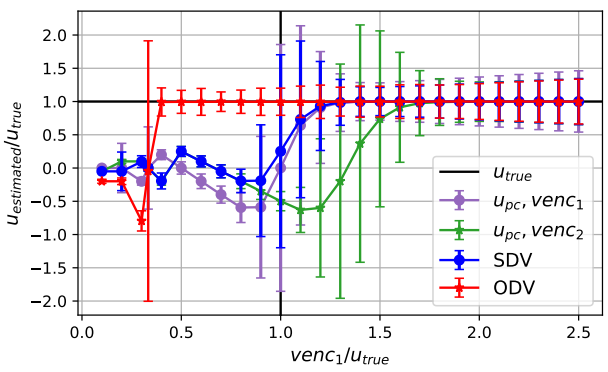

(c) $\beta = 0.75$

Fig. 5. Synthetic data (20% noise): single- and dual-VENC.

due to the nondesirable effect of overlapping of the single-VENC least squares functions mentioned in Section II-E. A similar, but less pronounced effect, occurs with $\beta = 0.75$. Therefore, in the real data acquisitions we continue using only $\beta = 0.66$ and $\beta = 0.75$.

B. Phantom data

The results for the phantom experiments are presented in Figure 6. The peak velocity in the tube is about 120 cm/s, what can be inferred from the single-VENC image with $\text{VENC}_1 = 150$. The wall of the tube can be distinguish as the noise ring separating the flow and the surrounding zero-velocity fluid. We first show the single-VENC PC-MRI, where aliasing for the two smaller VENCs can be clearly appreciated. We also confirm that SDV cannot handle the aliasing when both VENC values are lower than the true velocity, while ODV is able to sucessfully reconstruct un-aliased images from two aliased ones.

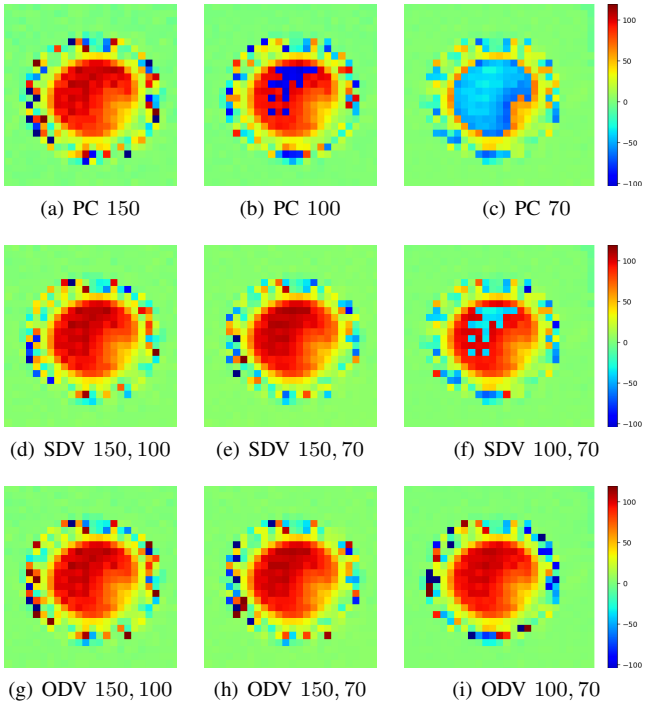

(a) PC 150 (b) PC 100 (c) PC 70

(d) SDV $150, 100$ (e) SDV $150, 70$ (f) SDV $100, 70$

(g) ODV $150, 100$ (h) ODV $150, 70$ (i) ODV $100, 70$

Fig. 6. Phantom data: single- (PC) and dual-VENC.

C. Volunteers data

Figure 7 presents the velocity profiles on the descending aorta for the different VENC combinations and different reconstruction methods for Volunteer 6. The figures for all the volunteers can be found in the Supplementary Material.

In all volunteers it is confirmed that ODV is the most robust method when decreasing the VENC, allowing to reconstruct velocities using lower VENCs than the true velocity, in contrast to SDV. Moreover, the theory is verified: aliasing is practically inexistent for $(\text{VENC}_1, \text{VENC}_2) = (50, 37.5)$ ($\beta = 0.75$), while aliasing always occurs at $(50, 33.3)$ ($\beta = 0.66$). Indeed, the peak velocity is approximately 130 cm/s, for $\beta = 0.75$, $\text{VENC}_1 = 50 > 130/3 \approx 40$, hence no aliasing appears. For $\beta = 0.66$, $\text{VENC}_1 = 50 < 130/2 \approx 65$, hence aliasing appears. The actual noise level of the acquisition seems to not affect the performance of the ODV.

Figure 8 summarises the ODV results for all volunteers when varying the VENC. The error is computed in terms of the ℓ^2-norm for the voxels inside the lumen, relative to the ℓ^2-norm of the reference image (average of VENC 150 cm/s with 3 repetitions).

V. Discussion

In this work, we present a method for reconstructing velocities using dual-VENC images, for the first time in the literature when both single-VENC images are aliased. The main advantage of the method is that the true velocity does not need be know exactly in advance, since alias is allowed for both VENCs. All previous works have proposed to unwrap low-VENC images using high-VENC images without aliasing [7], [8], [9], [3], [10]. The theoretical findings are confirmed in real data sets from an experimental phantom and volunteers.

The choice of the VENC's ratio $\beta = 0.66$ is the most robust to noise, independent on the MRI scanner settings. However, for the volunteers scanned here, $\beta = 0.75$ works satisfactory and therefore it allows lower aliasing limits for the ODV estimations than $\beta = 0.66$, as given by the theory. Let us recall that β can be kept fixed (for instance, optimized once for typical scan settings), while the scanner user only needs to choose VENC_1 as in a single-VENC acquisition.

Note that unwrapping methods using contiguous voxels - like the ones from [11] - can be still applied after the estimation with ODV. The unwrapping would then probably perform better due to the larger periods of the candidate solutions, e.g. $L_\Sigma = 6\text{VENC}_1$ for $\beta = 0.75$ and $L_\Sigma = 4\text{VENC}_1$ for $\beta = 0.667$.

Concerning the limitations of our study, the method was not assessed in patients, only in volunteers. It is well known that dual-venc approaches (as any other cardiovascular MRI sequences) are challenging due to variabilities during the experiment (not only measurment noise) [7], such as cardiac rhythm changes and subjects' motion. However, this variability will impact in similar manner the standard dual-VENC approach as well as the method proposed here. Another limitation is that data acquisition was performed for the two VENCs in a serial fashion, and therefore MRI scan protocols tailored to the ODV reconstructions have to be developed yet. This could be also done by including k-space undersampling techniques as in [8], what would allow dual-VENC protocols comparable in scan time to single-VENC ones, what is of high interest for the application of ODV to 4Dflow. Moreover, as in standard PC-MRI, there is the implicit assumption that the velocity is constant in space and time and therefore, neither the single- nor the dual-VENC approaches count for effects like dephasing of spins and turbulence.

VI. Conclusion

We present a robust method for estimating velocities from dual-VENC data in PC-MRI. The main contribution of this work is that both a theoretical and an extensive empirical analysis was carried out, turning out that there are high- and low-VENC combinations that can considerably reduce the aliasing issues. For example, in the volunteer data the ODV allows to choose the high-VENC up to a third of the maximal velocity. In clinical practice, the scanner operator has only to choose a single expected velocity, as for standard single-VENC PC-MRI. Then, the low-VENC value can be automatically fixed by the scanner in terms of the high-VENC. Moreover, the reconstruction method is simple enough to be implemented directly in the MRI scanner. Next steps are to assess the ODV in cases with high velocity variability, like stenotic vessels or valves, and 4Dflow, and application to other phase-contrast techniques, like elastography.

Acknowledgment

H.C. was supported by CONICYT-Doctorado nacional 21151645. C.B and A.O. acknowledge the funding of Conicyt

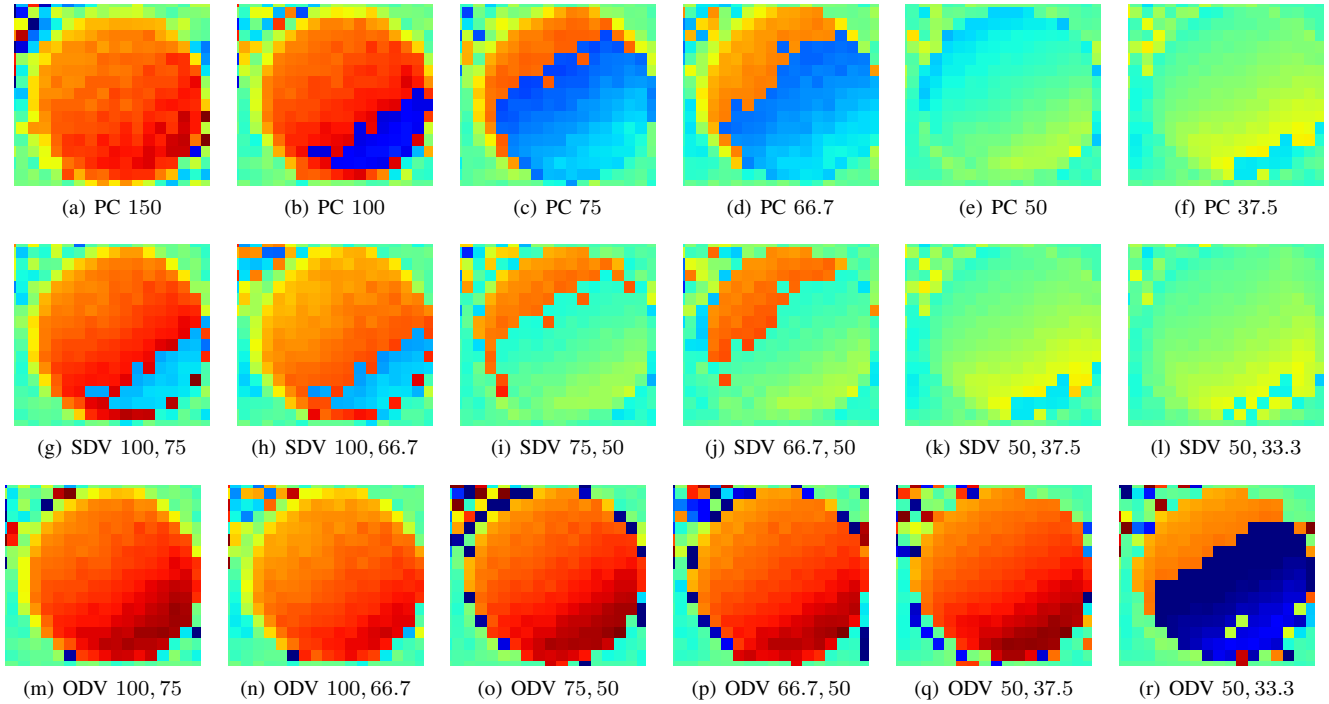

(a) PC 150 (b) PC 100 (c) PC 75 (d) PC 66.7 (e) PC 50 (f) PC 37.5

(g) SDV $100, 75$ (h) SDV $100, 66.7$ (i) SDV $75, 50$ (j) SDV $66.7, 50$ (k) SDV $50, 37.5$ (l) SDV $50, 33.3$

(m) ODV $100, 75$ (n) ODV $100, 66.7$ (o) ODV $75, 50$ (p) ODV $66.7, 50$ (q) ODV $50, 37.5$ (r) ODV $50, 33.3$

Fig. 7. Volunteer 6. First row: single-VENC PC-MRI. Second row: SDV. Third row: ODV. Velocities are coloured as in Figure 6.

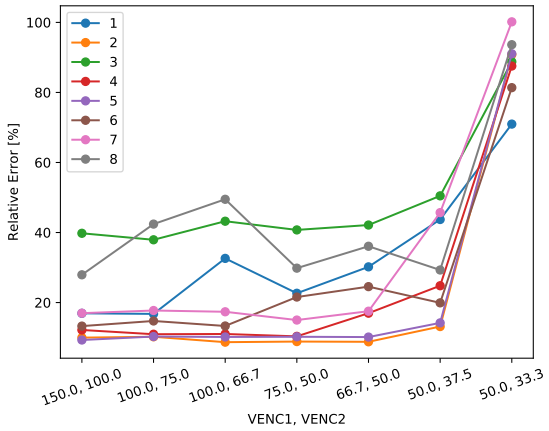

Fig. 8. Volunteers 1 to 8: $(\text{VENC}_1, \text{VENC}_2)$ v/s relative error between ODV and reference.

Basal Program PFB-03, and A.O. Fondecyt 1151512 and Fondap CR2-1511009. A.O and S.U. acknowledge funding from Millenium Science Initiative of the Ministry of Economy, Development and Tourism, grant Nucleus for Cardiovascular Magnetic Resonance. S.U. also thanks to Fondecyt 1181057.

References

[1] M. Srichai, R. Lim, S. Wong, and V. Lee, "Cardiovascular applications of phase-contrast mri," American Journal of Roentgenology, vol. 192, no. 3, pp. 662–675, 2009.

[2] P. Dyverfeldt, M. Bissell, A. J. Barker, A. F. Bolger, C.-J. Carlhäll, T. Ebbers, C. J. Francios, A. Frydrychowicz, J. Geiger, D. Giese, M. Hope, P. Kilner, S. Kozerke, S. Myerson, S. Neubauer, O. Wieben, and M. Markl, "4d flow cardiovascular magnetic resonance consensus statement," Journal of Cardiovascular Magnetic Resonance, vol. 17, p. 72, 2015.

[3] F. Callaghan, R. Kozor, A. Sherrah, M. Vallely, D. Celermajer, G. Figtree, and S. Grieve, "Use of multi-velocity encoding 4d flow mri to improve quantification of flow patterns in the aorta," Journal of Magnetic Resonance Imaging, vol. 43, no. 2, pp. 352–363, 2016.

[4] S. E. Petersen, B. A. Jung, F. Wiesmann, J. B. Selvanayagam, J. M. Fr̃ancis, J. Hennig, S. Neubauer, and M. D. Robson, "Myocardial tissue phase mapping with cine phase-contrast mr imaging: regional wall motion ana lysis in healthy volunteers." Radiology, vol. 238, no. 3, pp. 816–826, Mar 2006. [Online]. Available: http://dx.doi.org/10.1148/radiol.2383041992

[5] S. Hirsch, I. Sack, and J. Braun, Magnetic resonance elastography: physical background and medical applications. John Wiley & Sons, 2017.

[6] M. Loecher, E. Schrauben, K. Johnson, and O. Wieben, "Phase unwrapping in 4d mr flow with a 4d single-step laplacian algorithm," Journal of Magnetic Resonance Imaging, vol. 43, no. 4, pp. 833–842, 2016.

[7] A. Lee, B. Pike, and N. Pelc, "Three-point phase-contrast velocity measurements with increased velocity-to-noise ratio," Magnetic Resonance in Medicine, vol. 33, pp. 122–128, 1995.

[8] E. Nett, K. Johnson, A. Frydrychowicz, A. Muñoz, E. Schrauben, C. Francois, and O. Wieben, "Four-dimensional phase contrast mri with accelerated dual velocity encoding," Journal of Magnetic Resonance Imaging, vol. 35, no. 6, pp. 1462–1471, 2012.

[9] H. Ha, G. B. Kim, J. Kweon, Y.-H. Kim, N. Kim, D. H. Yang, and S. J. Lee, "Multi-venc acquisition of four-dimensional phase-contrast mri to improve precision of velocity field measurement," Magnetic resonance in medicine, vol. 75, no. 5, pp. 1909–1919, 2016.

[10] S. Schnell, S. Ansari, C. Wu, J. Garcia, I. Murphy, O. Rahman, A. Rahsepar, M. Aristova, J. Collins, J. Carr, and M. Markl, "Accelerated dual-

venc 4d flow mri for neurovascular applications," Journal of Magnetic Resonance Imaging, vol. 46, pp. 102–114, 2017.

[11] M. Loecher and D. Ennis, "Velocity reconstruction with nonconvex optimization for low-velocity-encoding phase-contrast mri," Magnetic resonance in medicine, 2017.

[12] J. Urbina, J. Sotelo, D. Springmüller, C. Montalba, K. Letelier, C. Tejos, P. Irarrázaval, M. Andia, R. Razavi, I. Valverde, and S. Uribe, "Realistic aortic phantom to study hemodynamics using mri and cardiac catheterization in normal and aortic coarctation conditions," Journal of Magnetic Resonance Imaging, vol. 44, no. 3, pp. 683–697, 2016.

[13] C. Montalba, J. Urbina, J. Sotelo, M. Andia, C. Tejos, P. Irarrazaval, D. Hurtado, I. Valverde, and S. Uribe, "Variability of 4d flow parameters when subjected to changes in mri acquisition parameters using a realistic thoracic aortic phantom," Magnetic resonance in medicine, 2017.

[14] M. Bernstein, M. Grgic, T. Brosnan, and N. Pelc, "Reconstructions of phase contrast, phased array multicoil data," Magnetic resonance in medicine, vol. 32, no. 3, pp. 330–334, 1994.

[15] M. A. Bernstein, A. Shimakawa, and N. J. Pelc, "Minimizing te in moment-nulled or flow-encoded two-and three-dimensional gradient-echo imaging," Journal of Magnetic Resonance Imaging, vol. 2, no. 5, pp. 583–588, 1992.

[16] R. W. Brown, Y.-C. N. Cheng, E. M. Haacke, M. R. Thompson, and R. Venkatesan, Magnetic Resonance Imaging: Physical Principles and Sequence Design. John Wiley & Sons, 2014.